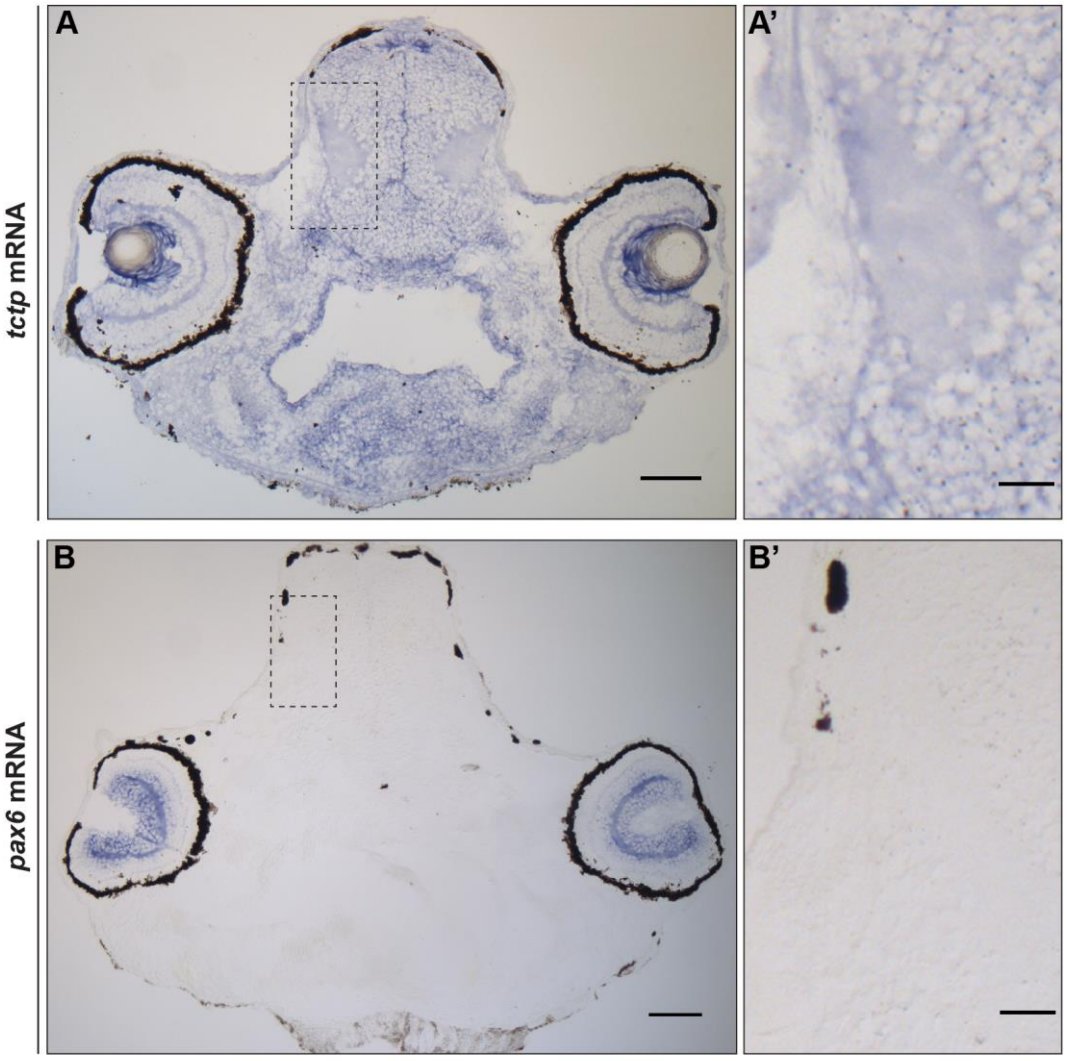

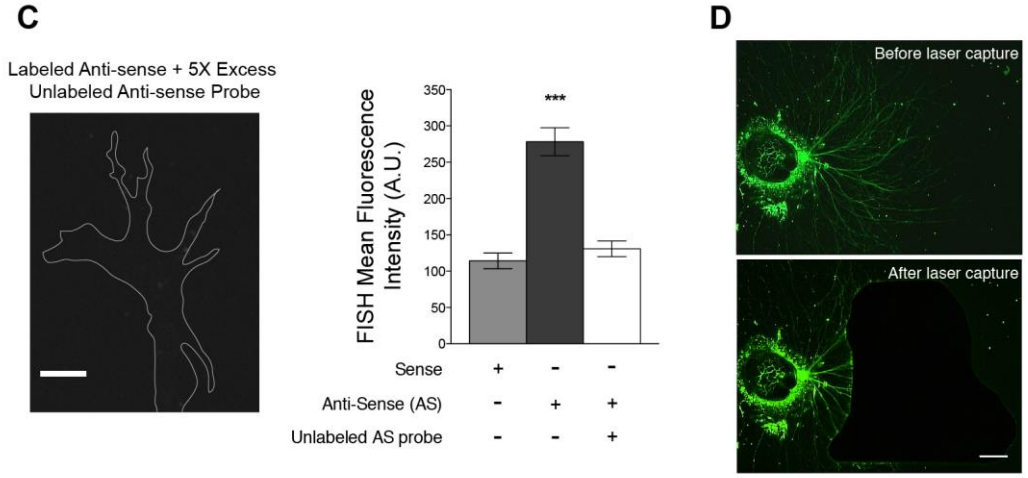

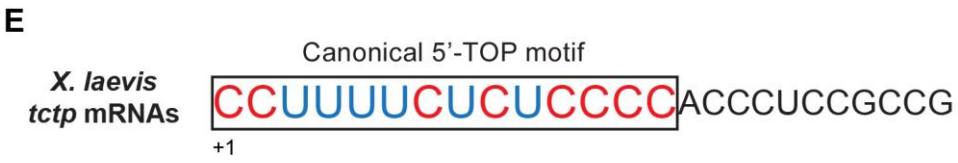

Figure S1. *tctp* mRNA expression in the developing frog embryo. (A and B) *In situ* hybridization detection of *tctp* and *pax6* mRNA expression on coronal sections of stage 43 embryos. The boxed areas, which mark the lateral surface of the mesencephalon through where retinal ganglion cell axons pass en route to the optic tectum, their synaptic target, are shown at a higher amplification in (A') and (B'). (C) Continues Fig. 1D,E: Quantitative *in situ* hybridization detection of *tctp* mRNA expression in the RGC axonal and growth cone compartments was performed using stage 32 eye explants grown *in vitro* for 24 hours. Here, an additional control is shown – the hybridization signal obtained with labelled *tctp* mRNA was eliminated by competition using an 5:1 excess amount of unlabelled *tctp* antisense oligonucleotide probes. Quantification of mean fluorescence intensity is also presented (mean ± SEM; *** $P < 0.0001$, one-way ANOVA and Bonferroni); 'sense' fluorescence signal was used for normalization purposes. (D) Micrographs of the laser-capture microdissection procedure. (E) First 25 nucleotides of the *Xenopus laevis tctp* 5'UTR. As noted, the 5'UTR of *tctp* transcripts starts with a canonical 5'-terminal oligopyrimidine (TOP) motif, a typical feature of transcripts selectively regulated at the translational level by mTORC1. Scale bars: 100 μm in (A) and (B), 5 μm in (C), 200 μm in (D).

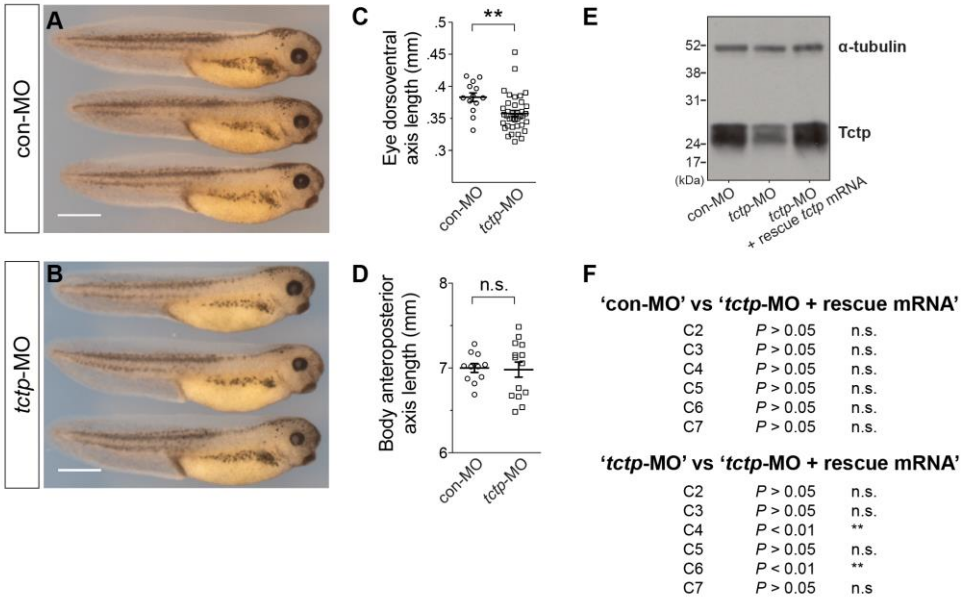

F

'con-MO' vs '*tctp*-MO + rescue mRNA'

C2	$P > 0.05$	n.s.
C3	$P > 0.05$	n.s.
C4	$P > 0.05$	n.s.
C5	$P > 0.05$	n.s.
C6	$P > 0.05$	n.s.
C7	$P > 0.05$	n.s.

'*tctp*-MO' vs '*tctp*-MO + rescue mRNA'

C2	$P > 0.05$	n.s.
C3	$P > 0.05$	n.s.
C4	$P < 0.01$	**
C5	$P > 0.05$	n.s.
C6	$P < 0.01$	**
C7	$P > 0.05$	n.s

G

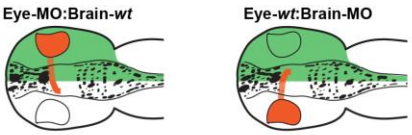

Kruskal-Wallis test

P-value	0,0002 (Gaussian Approximation)
P-value summary	***
Do the medians vary significantly ($P < 0.05$)?	Yes
Number of groups	4
Kruskal-Wallis statistic	19,27

Dunn's Multiple Comparison Test

	Difference in rank sum	Significant? $P < 0.05$?	Summary
A vs. B	22,08	Yes	**
A vs. C	4,375	No	n.s.
A vs. D	2,911	No	n.s.
B vs. C	17,7	Yes	*
B vs. D	-19,17	Yes	**
C vs. D	-1,464	No	n.s.

Eye-MO:Brain-*wt*: con-MO (A) vs. *tpt1*-MO (B)

Eye-*wt*:Brain-MO: con-MO (C) vs. *tpt1*-MO (D)

Figure S2. Morphological characterization of Tctp knockdowns. (A and B) Micrographs of stage 39 con-MO- or *tctp*-MO-injected embryos. Albeit with smaller eyes, Tctp morphants appear morphologically normal, and their development progresses at comparable rates relative to con-MO-injected tadpoles. (C) Plot of eye size measurements (mean ± SEM; ** $P < 0.0063$, unpaired *t*-test). (D) Plot of body length (anteroposterior axis) measurements (mean ± SEM; n.s. $P < 0.8614$, unpaired *t*-test). (E) The normalization of Tctp protein expression levels was evaluated by Western blot after a morpholino-resistant *tctp* transgene was co-injected with *tctp*-MO. Protein extracts were prepared from stage 37/38 embryos. (F) Complements Fig. 2I: Summary of the statistical analysis examining the effect of normalizing Tctp expression levels on the development of Tctp-depleted projections. (G) Complements Fig. 3D-H: Summary of the statistical analysis performed to evaluate the impact of Tctp deficiency on the length of the retinotectal projection. Scale bars: 110 µm.

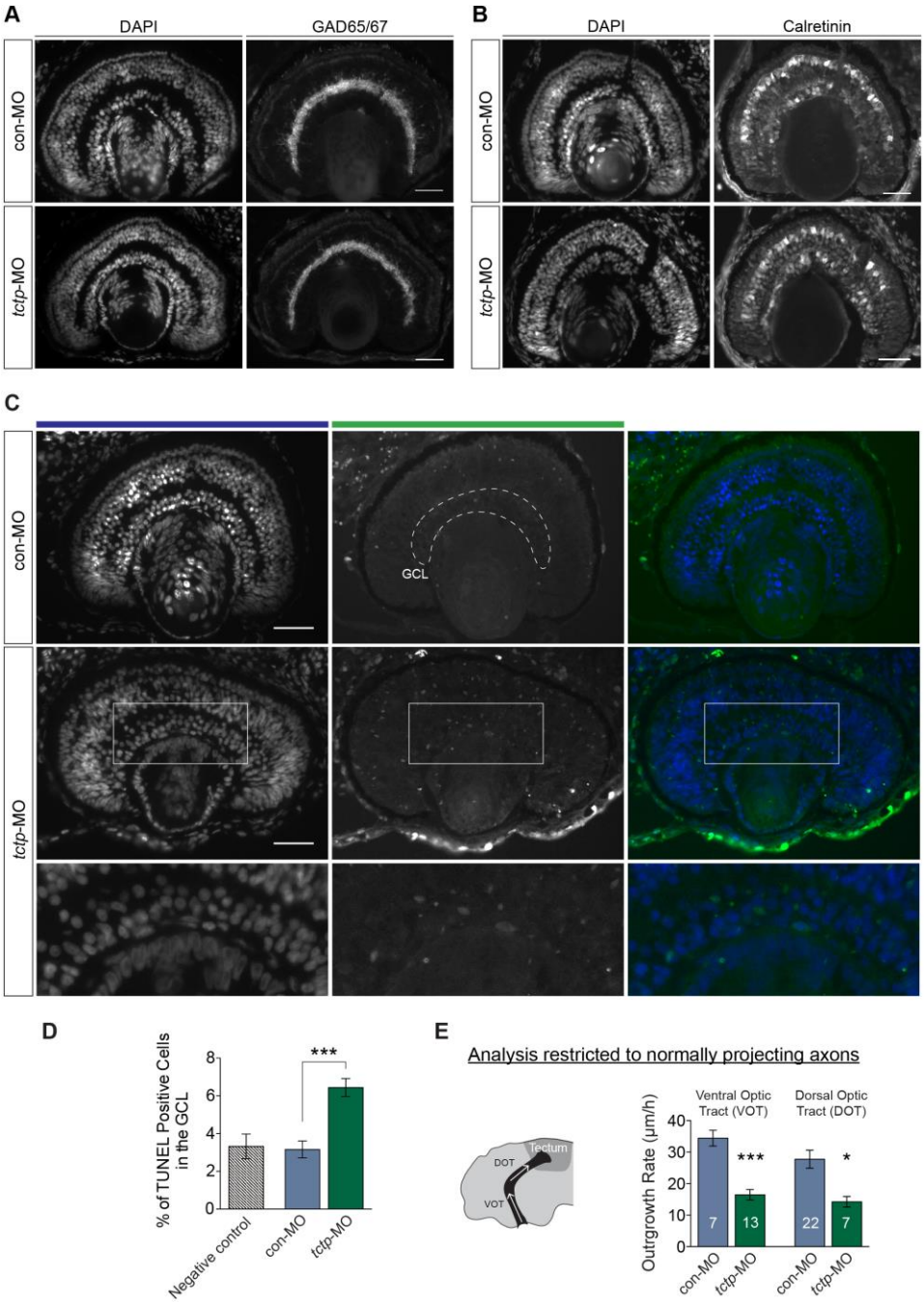

Figure S3. Tctp deficiency impairs axon extension *in vivo*. (A and B) Coronal sections of stage 43 control or Tctp-depleted retinas probed for Glutamate decarboxylase (GAD65/67) and Calretinin, two cell-type-specific markers (GAD65/67 and Calretinin antisera detect GABAergic amacrine cells, and retinal ganglion cell/bipolar cells, respectively). (C and D) TUNEL staining on stage 43 control or Tctp-depleted retinas. The number of TUNEL-positive cells in the ganglion cell layer was found to be increased in Tctp morphants (mean ± SEM; $n > 30$ embryos for both backgrounds; *** $P < 0.0001$, unpaired *t*-test). (GCL: ganglion cell layer, approximated by the dashed outline). The boxed areas are shown at a higher amplification in the bottom panels. (E) Plot showing the average extension rates measured from time-lapse recordings of RGC axons coursing normally (i.e. without guidance errors) through the ventral optic tract (VOT) and dorsal optic tract (DOT) in controls and Tctp morphants (mean ± SEM; n = no. of axons analysed; VOT: *** $P < 0.0001$, unpaired *t*-test; DOT: * $P < 0.0159$, unpaired *t*-test). Scale bars: 50 µm.

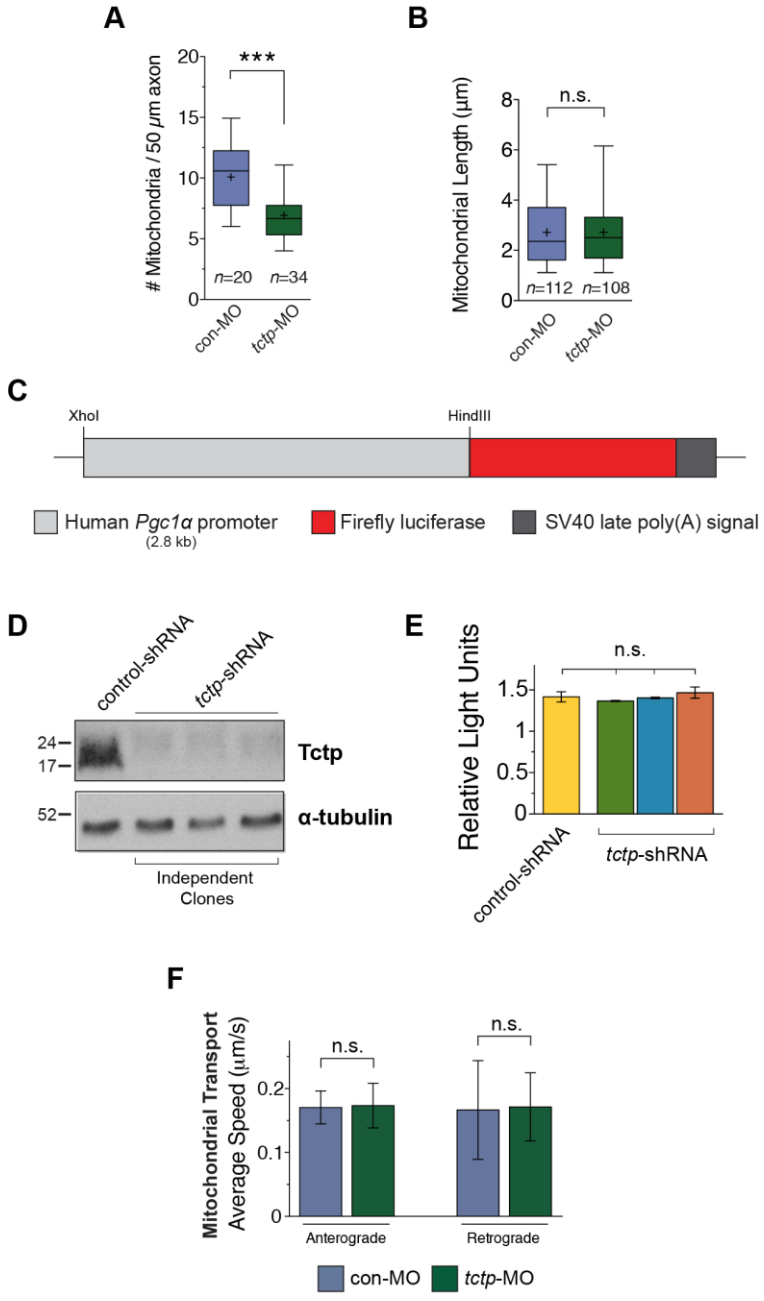

Figure S4. Tctp knockdown compromises axonal mitochondrial function. (A) Stage 32 control and Tctp morphant eye explants were grown *in vitro* for 24 hours and incubated with MitoTracker to visualize mitochondria. The plot shown here represents the average number of axonal mitochondria found in con-MO- or *tctp*-MO-positive retinal ganglion cells (boxplot: whiskers cover 5-95 percentile, '+' denotes the mean value; n = no. of axons analysed; *** $P < 0.0001$, Mann-Whitney test). (B) Plot of axonal mitochondrial length in control and Tctp-depleted retinal ganglion cells (boxplot: whiskers cover 5-95 percentile, '+' denotes the mean value; n = no. of axons analysed; n.s., $P = 0.7960$, Mann-Whitney test). (C-E) Normal *pgc1a* expression in HCT116 cells deficient for Tctp. The rational for applying this seemingly indirect approach is not immediate. We knew *a priori* that basal P53 levels were elevated in *tctp*$^{+/-}$ mice (Amson et al., 2012) and that the expression of *pgc1a* was repressed by the activation of P53 in the context of telomere dysfunction (Sahin et al., 2011). Since the mitochondrial traits identified in Tctp morphants were reminiscent of dysfunctional Pgc1α activity (Wareski et al., 2009), we hypothesised that the activation of P53 in Tctp-deficient backgrounds could result in mitochondrial dysfunction due to its

repression of *pgc1a* expression. Hence the strategy used here, for it allowed us to evaluate the expression of *pgc1a* at the transcriptional level. (C) The promoter region of human *pgc1a* (2.8 kb) was cloned upstream of the luciferase gene cassette and stably transfected into *tctp* or control shRNA-infected HCT116 cells. Subsequently, lysates of *tctp* or control shRNA-infected HCT116 cells were run on a SDS-PAGE gel and Tctp protein expression verified by western blot. Tctp expression knockdown was as high as 85% in these cells (D). We show in (E) a plot of the average relative light units (RLU) measured in cells co-transfected with *pgc1a*-luc and a control plasmid (mean ± SEM; six biological replicates of *tctp*-shRNA-infected cells were measured in triplicate in the two independent rounds of experiments conducted; *** $P = 0.5544$, one-way ANOVA). (F) Quantitative analysis of mitochondrial transport velocities. Population-wide study of mitochondrial velocities (excluding stationary organelles) suggests that no significant differences exist between control and Tctp-depleted axons, in agreement with the dataset shown in Fig. 7I (mean ± s.e.m.; anterograde direction: n.s., $P = 0.9941$; retrograde direction: n.s., $P = 0.9371$; statistical analyses used Mann-Whitney test).

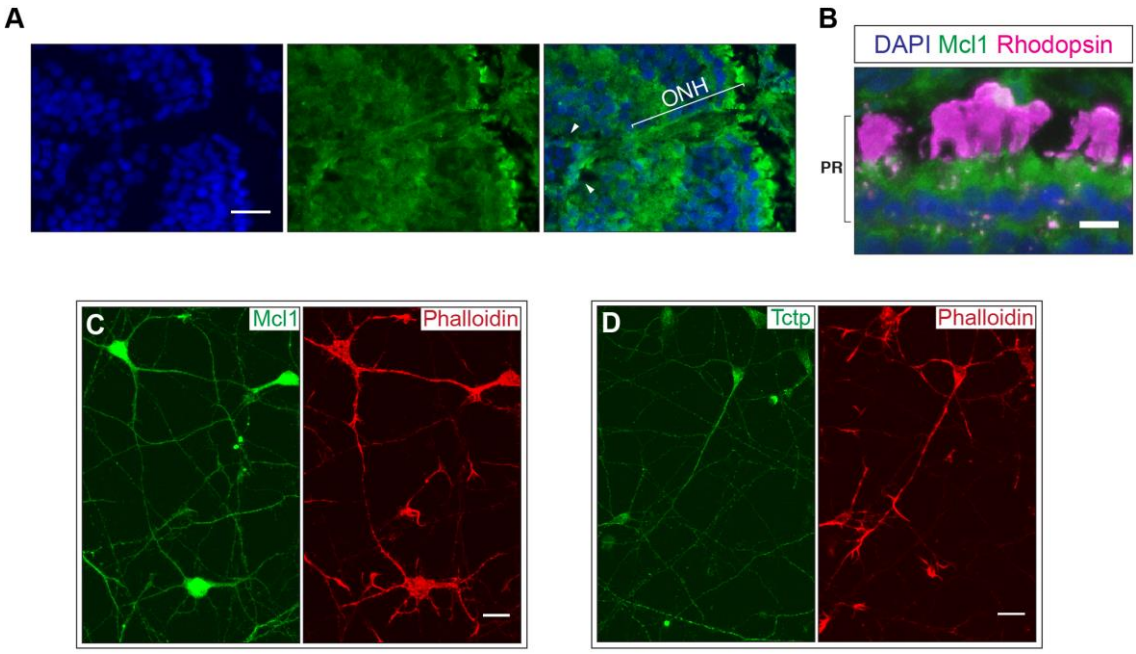

Figure S5. Pro-survival Mcl1 is expressed in the axonal compartment. (A) Complements Fig. 8A: Optic nerve head (ONH) region of a stage 43 wild-type retina (coronal section) probed for Mcl1 and counterstained with DAPI. Mcl1 was detected in the optic fiber layer and the optic nerve head, indicating that, like Tctp, this protein localizes to retinal ganglion cell axons in *vivo*. (B) Complements Fig. 8A: Outer nuclear layer of a stage 43 wild-type retina (coronal section) probed for Mcl1 and Rhodopsin, and counterstained with DAPI. Similar to Tctp, Mcl1 was detected in the inner segment of photoreceptors. (C and D) Cultured rat cortical neurons (E18.5 + 3DIV) stained for Mcl1 or Tctp, and counterstained with Phalloidin. Scale bars: 25 µm in (A), (C) and (D), 10 µm in (B).

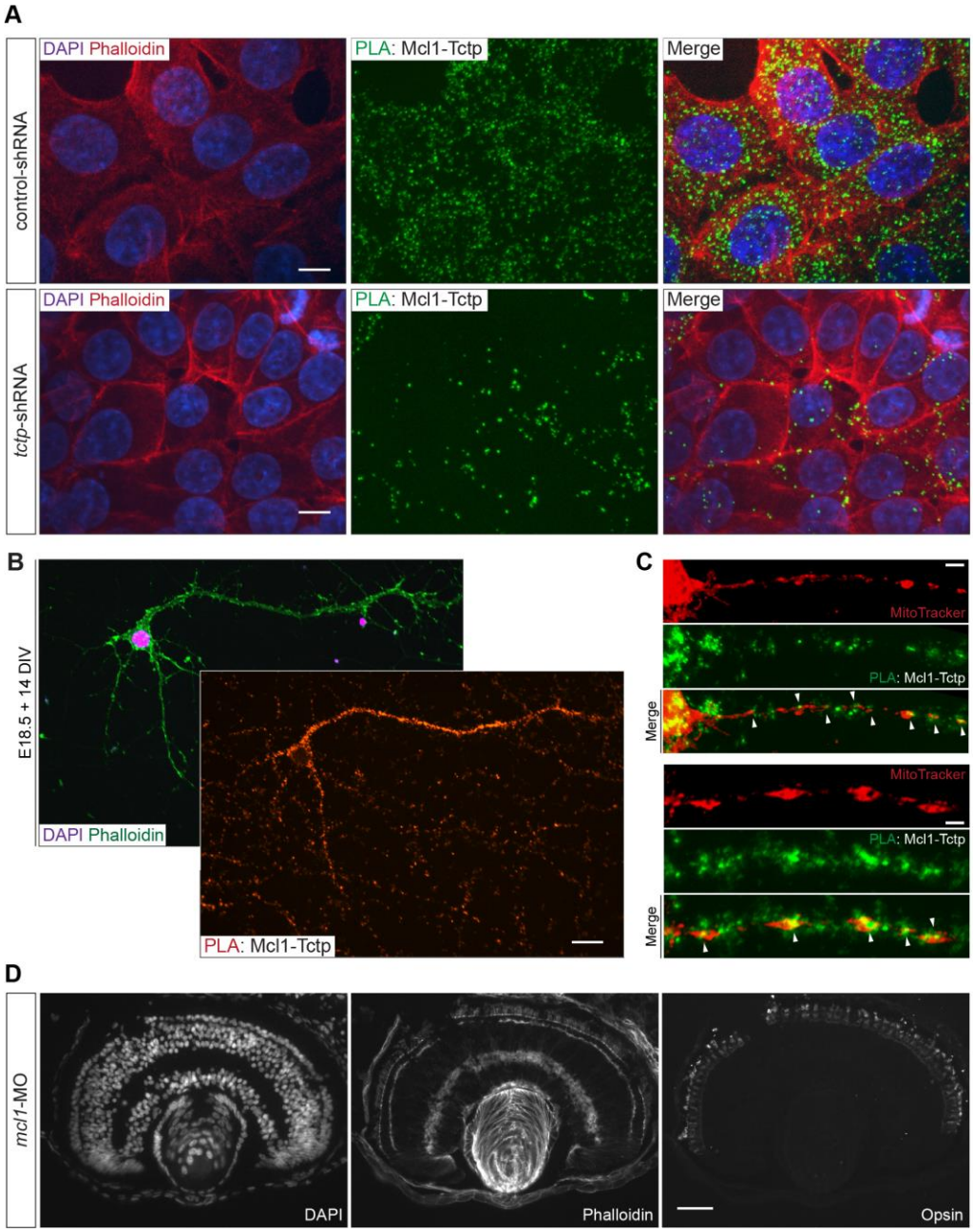

Figure S6. Axonal Tctp interacts with pro-survival Mcl1. (A) PLA signal (green) obtained using anti-Tctp and anti-Mcl1 sera in control- or *tctp*-shRNA-infected HCT116 cells, counterstained with DAPI (blue) and phalloidin (red). (B) PLA signal obtained using anti-Tctp and anti-Mcl1 sera in cultured rat cortical neurons (E18.5 + 14 DIV), counterstained with DAPI and phalloidin. (C) PLA signal obtained using anti-Tctp and anti-Mcl1 sera in cultured rat cortical neurons (E18.5 + 3 DIV), counterstained with MitoTracker. Arrowheads denote PLA positive puncta co-localizing with mitochondria. The bottom three panels are centred on a distal region of the neurite. The data indicates that approximately 5-10% of Tctp-Mcl1 PLA puncta co-localize with mitochondria in neurites. This is in agreement with observations by Yang and colleagues who found by immunocytochemistry means that Tctp and Bcl-X_L partially co-localize not only in mitochondria but also in the cytosol (Yang et al., 2005). It is noteworthy that while anti-apoptotic Bcl-2 family proteins are generally integrated within the outer mitochondrial membrane, they can also be found in the cytosol or in the endoplasmic reticulum membrane (Chipuk et al., 2010). Furthermore, pro-apoptotic Bax, whose homodimerization in the outer mitochondrial membrane is prevented by Tctp

(Susini et al., 2008), is usually cytosolic (Chipuk et al., 2010). Likewise, the cellular localization of Tctp is mainly cytoplasmic in healthy cells (Bommer and Thiele, 2004; Gachet et al., 1999; Yang et al., 2005). One possibility is that Tctp shuttles between the cytosol and the outer mitochondrial membrane in non-apoptotic conditions. (D) Stage 43 Mcl1-depleted retina probed with anti-Opsin antibody, counterstained with phalloidin and DAPI. Signs of morphological disruption were not detected on examination of the retina in Mcl1 morphants, suggesting that the *mcl1*-MO does not elicit widespread toxicity. Scale bars: 5 µm in (A), 10 µm in (B) and (C), 50 µm in (D).

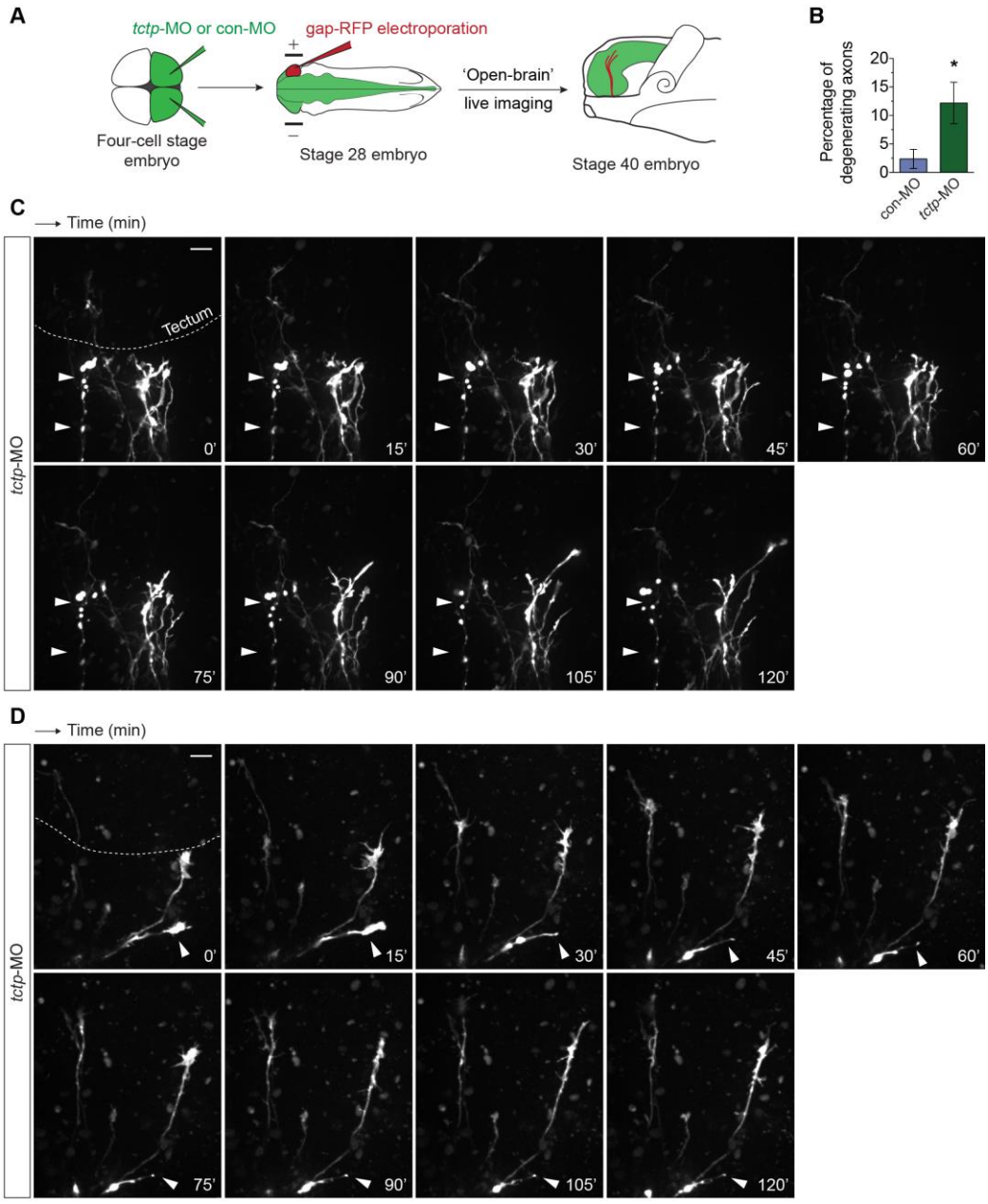

Figure S7. Degenerating retinal ganglion cell axons in Tctp morphant projections. (A) Schematic representation of the experiment. con-MO- or *tctp*-MO-injected stage 28 embryos were electroporated with gap-RFP to label retinal axons and allowed to develop until stage 40 before *in vivo* brain imaging. (B) Percentage of retinal ganglion cell axons classified as degenerating in controls and Tctp morphants (mean ± SEM; n = no. of axons analysed; * $P < 0.0418$, unpaired t-test). (C) Time-lapse images of Tctp-depleted retinal ganglion cell axons coursing through the optic tract. Dashed lines indicate the boundary of the optic tectum. Arrowheads indicate a degenerating axon, as suggested by its beaded morphology. Note that this axon has not yet reached the optic tectum; thus, it is unlikely that such effect is elicited by normally occurring pruning mechanisms. (D) Time-lapse images of Tctp-depleted retinal ganglion cell axons coursing through the optic tract. Dashed lines indicate the boundary of the optic tectum. Arrowhead indicates a degenerating axon with a retracting behaviour. Scale bars: 10 µm.

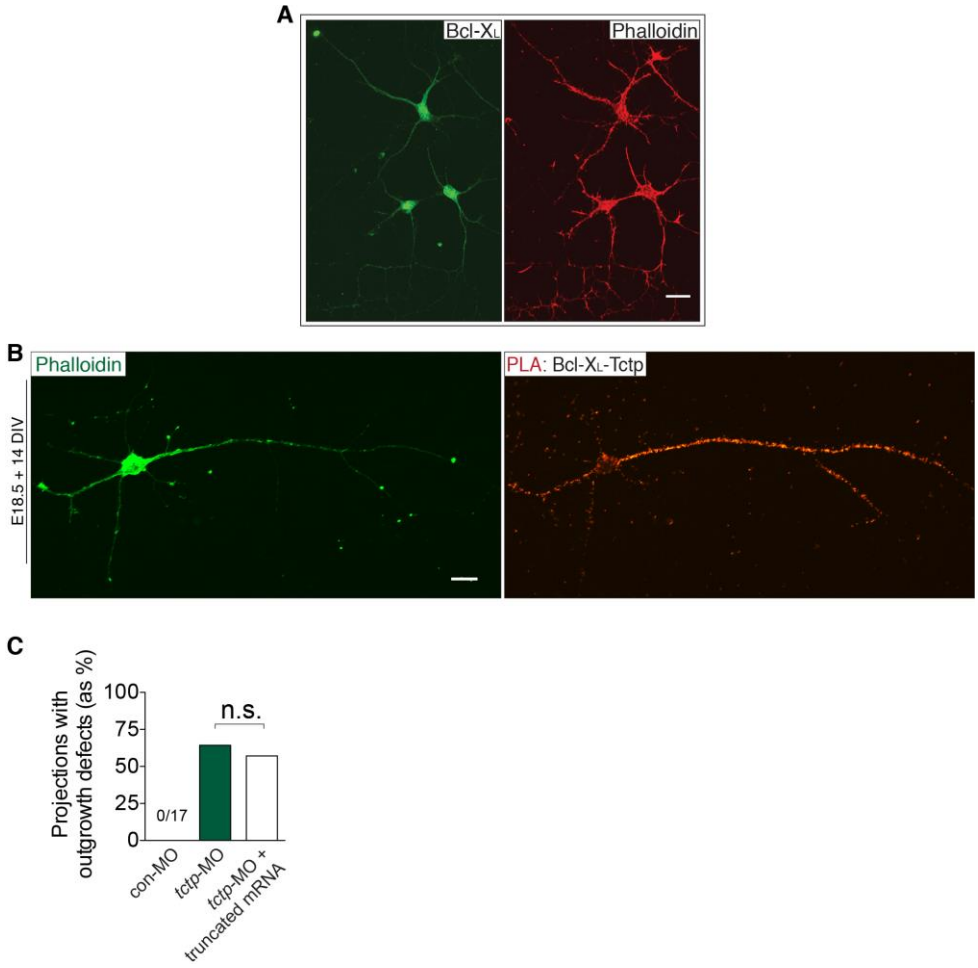

Figure S8. Axonal Tctp interacts with Mcl1-related Bcl-XL. (A) Cultured rat cortical neurons (E18.5 + 3DIV) stained for Bcl-X_L, and counterstained with Phalloidin. (B) PLA signal obtained using anti-Tctp and anti- Bcl-X_L sera in cultured rat cortical neurons (E18.5 + 14 DIV), counterstained with DAPI and phalloidin. (C) Co-delivery of *tctp*-MO and *tctp*$_{40\text{-}172}$ mRNA, encoding a truncated Tctp protein devoid of anti-apoptotic activity, fails to rescue the effects of Tctp depletion on the development of the retinotectal projection. Number of embryos displaying axon extension defects ('*tctp*-MO' versus '*tctp*-MO + *tctp*$_{40\text{-}172}$ mRNA': n.s., $P = 1.00$; Fisher's exact test, performed on number of observations but plotted as percentages). Scale bars: 25 µm in (A), 10 µm in (B).

SUPPLEMENTARY MATERIALS AND METHODS

Immunostaining of retinal sections

Anesthetized embryos were fixed in 4% paraformaldehyde (vol/vol) in phosphate buffered saline (PBS) overnight at 4ºC, washed, and incubated in 30% sucrose (wt/vol) in PBS for 2 hours at 4ºC before sectioning. Transverse 12-µm cryosections were processed using standard immunohistochemistry protocols (blocking solution: 10% heat-inactivated goat serum, 1% bovine serum albumin, 0.5% Triton X-100 in 1X PBS). Antibodies: rabbit anti-Tctp (1:500, gift from J. Kubiak); mouse anti-Calbindin D-28k (1:1000, Swant; catalogue number 300); rabbit anti-Calretinin (1:1000, Millipore; AB5054); rabbit anti-GAD65/67 (1:200, Abcam; ab11070) mouse anti-Rhodopsin (1:200, Novus Biologicals; catalogue number NBP1-47602), mouse anti-Opsin (1:1000, Sigma; clone RET-P1), rabbit anti-Mcl1 (1:200; gift from Y. Tsuchiya). Alexa Fluor 488 phalloidin (Life Technologies) was used at 1:40. Nuclei were labelled with 0.1 µg/mL DAPI (Life Technologies) during the last wash step before mounting. Alexa Fluor secondary antibodies (Life Technologies) were used at 1:1000. Antigen retrieval with steaming 0.01 M sodium citrate (0.05% Tween 20, pH 6.0) was carried out before staining for Tctp. Processed sections were visualized on a Nikon Eclipse 80i microscope and photographed with a Hamamatsu ORCA-ER camera.

In situ hybridization (ISH) and fluorescent _in situ_ hybridization (FISH)

In situ hybridization on transverse cryosections of fixed embryos was performed as described previously (Xue and Harris, 2012). Digoxigenin-labelled RNA probes were generated from linearized IMAGE clones (*tctp* IMAGE ID: 5542512; *cox5a* IMAGE ID: 4407278). Photomicrographs were taken with a Zeiss Axoskop microscope equipped with a Micropublisher 5.0 RTV camera (Qimaging). Signal intensity was measured by manually tracing the ganglion cell layer and the inner plexiform layer using Photoshop (Adobe). Intensity measurements were normalized to background signal (Love et al., 2014). FISH probe design followed documented guidelines (Bassell et al., 1998), and probes were 3'-labeled with DIG oligonucleotide tailing kit (Roche); FISH procedure on retinal growth cones was then carried out as described with minor variations (Zivraj et al., 2010). FISH antisense probe sequences in 5'-3' orientation: TAGATATCCGAGAACATTTCGTCTTCAGTGATGCAGTCCTTGTAGATGA, ATCATCAATTGCACCTTCTTCTCTTTGGATTACCTTGCCTTCAACTTC, CCTTATGTAATTCTTGTAAGAGTCCTTGGTGAAGCCTGTTTCCTGAA, GGGGTTCATTCTTTCTCCGGTGTAAAACTGATAGTTTTTGAAATTTCGAAG.

Laser-capture microdissection and RNA extraction

Per experiment, ~140 stage 33/34 eye explants were plated on polyethylene terephthalate membrane slides (Leica Microsystems), pre-coated with poly-L-lysine (10 µg/mL; Sigma) and laminin (10 µg/mL, Sigma), and cultured for 32-36 hours. As described previously (Zivraj et al., 2010), retinal cultures were fixed (4% paraformaldehyde, 4% sucrose in 1X PBS) for 10 minutes, subsequently dehydrated through an ethanol series, and air-dried before microdissection. To aid visualization, the membrane stain FM 1-43FX (Life Technologies) was added 20 minutes before fixation. Samples were processed using the Leica LMD6000 system. RNA was extracted with RNAqueous-Micro kit (Life Technologies) according to manufacturer's instructions. Unlike Zivraj et al., a linear

amplification step was not included before to RACE, RT-PCR or RT-qPCR analyses. Control RT-PCR reactions were performed using OneStep RT-PCR kit (QIAGEN). The presence of *map2*, *hist1h4a*, and *actb* transcripts was evaluated by RT-PCR before proceeding with further experiments. See Table 1 for oligonucleotide primer details.

Quantification of *tctp* mRNA isoforms by RT-qPCR

Eye and axonal RNA extracts were prepared as detailed above. QIAGEN QuantiTect SYBR Green RT-PCR kit was used with a Roche LightCycler 480 Real-Time PCR system. Manufacturer's guidelines were followed thoroughly except for primer concentration – 0.4 µM instead of 0.5 µM was found optimal. Primer design intently kept amplicon size below 150 base pairs to ensure optimal amplification efficiency. Due to the inexistence of introns in the 3'UTR of the *tctp* gene, it was impossible to design primers targeting the unique region of *tctp*-L and spanning an exon-intron boundary. Hence, when designing primers targeting the coding region of *tctp*, exon-intron boundaries were avoided. To minimize potential pipetting errors during the initial reaction assembly, each reaction was run in quadruplicate (10-µL reactions). Plates were centrifuged at 1,500 x *g* for 2 minutes at 4ºC before commencing the cycling protocol. Standard curves for the calculation of amplification efficiency were run independently from the actual experiments (Pfaffl, 2001). Relative quantification data was obtained following the comparative Ct method (Livak and Schmittgen, 2001) using Roche's LightCycler 480 data analysis module. *Actb* mRNA was used as reference for data normalization. As an additional quality control for the axonal RNA preparations the presence of *map2* and *hist1h4a* transcripts was evaluated by RT-PCR before running each RT-qPCR experiment. See Table 1 for oligonucleotide primer details.

Morpholino antisense oligonucleotides

Antisense *tctp*-MO (translation-blocking), *mcl1*-MO (splice-blocking), and control-MO were designed and supplied by GeneTools: 5'-ATCATGTTGGCGGCCTAAGTGTTGT-3', 5'-AGTAGAGTAAGCCATGCTCACCCGT-3', and 5'-CCTCTTACCTCAGTTACAATTTATA-3', respectively. Fluorescein-tagged (3'end) morpholinos were used throughout in *tctp*-targeting experiments, except when mt-GFP was to be subsequently electroporated.

In order to test the specificity of *tctp*-MO in respect to off-target effects, the synthesis of a morpholino-resistant rescue *tctp*-S-mimicking transgene was commissioned to a manufacturer of custom DNA products (GENEWIZ). Specifically, this rescue transgene had the *tctp* 5'UTR fragment targeted by the *tctp*-MO replaced by the corresponding *actb* fragment. The rescue experiments involved *in vitro* transcribed mRNAs produced from a plasmid containing this transgene co-delivered with *tctp*-MO by blastomere microinjection.

DiI labelling of retinal axons

As described (Leung et al., 2013), embryos were fixed overnight at 4 ºC in 4% paraformaldehyde in PBS; after a quick wash in PBS, RGC axons were labelled by intraocular injection of the fluorescent carbocyanine DiI (1,1'-dioctadecyl-3,3,3',3'-tetramethylindocarbocyanine perchlorate, Life Technologies). Dye crystals were dissolved in 100% ethanol and heated to 65 ºC for five minutes before use. Fourteen to twenty hours at 19-22 ºC were allowed to ensure the complete distribution of the dye before proceeding. Then, the contralateral (in respect to the dye-injected eye) brain hemisphere was dissected, mounted in 1X PBS and immediately visualized on an inverted laser-scanning confocal microscope (Olympus FV1000). Optic projection length was normalized to the distance between the optic chiasm and the posterior boundary of the optic tectum, two easily recognizable anatomical landmarks on bright-field/red-channel superimposed images. Each

measurement reflects the length of the longest axon and data were subsequently normalized against the mean projection length of the control group.

In vivo imaging of axon pathfinding

tctp-MO- or con-MO-injected embryos were electroporated with gap-RFP or gap-RFP and mt-GFP. Anesthetized embryos, selected on the basis of a healthy appearance, were restrained before the skin and dura were carefully removed above the contralateral optic tract. Specimens were then mounted in an imaging chamber consisting of two superimposed Gene Frame adhesive frames (Thermo) on oxygenated Permanox slides (Nunc). Images were acquired every 15 minutes for up to 2 hours using an UltraView VoX spinning disk confocal imaging system on an Olympus IX81 microscope, or a Nikon Eclipse TE2000-U or, alternatively, a Nikon Eclipse 80i setup. Axon outgrowth was analysed with Volocity (PerkinElmer); axons were scored as 'stalled' if their outgrowth was ≤ 10 μm over the 2-hour period of analysis. GFP-labelled mitochondria were imaged exclusively on an UltraView VoX spinning disk confocal imaging system on an Olympus IX81 microscope.

TUNEL assay – *in situ* cell death detection in the ganglion cell layer

Anesthetized embryos were fixed in 4% paraformaldehyde (vol/vol) in phosphate buffered saline (PBS) overnight at 4ºC, washed, and incubated in 30% sucrose (wt/vol) in PBS for 2 hours at 4ºC before sectioning. Stage 43 transverse 12- μm cryosections were washed in PBS (three 10-minute washes with gentle rocking), and subsequently incubated in permeabilization solution (PBS/0.5% Triton X-100; three 10-minute washes with gentle agitation). TUNEL labelling was performed following the instructions provided by the manufacturer (*In situ* Cell Death Detection Kit – TMR red, Roche). Nuclei were labelled with 0.1 μg/mL DAPI (Life Technologies) during the last wash step before mounting. The mixture used in negative labelling controls did not include the enzyme required to catalyse the addition of TMR red-dUTPs. Processed sections were visualized on a Nikon Eclipse 80i microscope and photographed with a Hamamatsu ORCA-ER camera. Data

measurements reflect, per section, the ratio between TUNEL-positive nuclei and the total number of DAPI-stained nuclei in the ganglion cell layer (plotted as percentage).

ATP bioluminescence assay

As documented (Agathocleous et al., 2012), paired retinas from stage 37/38 embryos were dissected in 1X Modified Barth's Saline containing ethyl 3-aminobenzoate methanesulfonate (0.04% wt/vol; Sigma). ATP content was measured with ATP bioluminescence kit CLS II (Roche) according to manufacturer's instructions on a Turner Designs luminometer, model TD-20/20. Immediately after dissection, single retinas were incubated in 50 µL of 1% perchloric acid for precisely 10 minutes at room temperature before the reaction was stopped in 450 µL of boiling Tris buffer (100 mM Tris, 4 mM EDTA, pH 7.75), incubated for 2 minutes at 100ºC, and centrifuged at 1,000 x *g* for 1 minute. The supernant was then transferred to a fresh tube and kept on ice until bioluminescence readings were taken. For each tadpole, the total protein content of the 'second' retina was measured on a Qubit 2.0 Fluorometer (Life Technologies) following manufacturer's recommendations; protein lysates were prepared in ice-cold (150 mM NaCl, 1% NP-40, 0.5% sodium deoxycholate, 0.1% SDS, 50 mM Tris, pH 8.0) by sonication. Experimental ATP values were interpolated from a standard curve and normalized to total protein.

Mitochondrial membrane potential ($\Delta\Psi_m$) measurement

Retinal cultures were incubated with 20 nM tetramethylrhodamine, methyl ester (TMRM) at 20ºC for 20 minutes and washed with pre-warmed culture medium before imaging on a Nikon Eclipse TE2000-U microscope. To reduce phototoxicity, lamp fluorescence was limited to 25% and a 0.9 neutral density filter was used. To account for the dependence of F_m on $\Delta\Psi_p$, a corrected value for $\Delta\Psi_m$ was derived from the ratio of fluorescence intensities between mitochondria (F_m) and mitochondria-poor regions along the axon and in the growth cone (F_c) (Marks et al., 2005).

Fluorescence measurements were taken by manually tracing mitochondria using Volocity (PerkinElmer); the mitochondria-rich growth cone central domain was analysed as a single element.

Visualizing mitochondrial dynamics

Con-MO- or *tctp*-MO-positive retinal explants were incubated with 25 nM MitoTracker Red, a mitochondrion-selective probe, at 20ºC for 20 minutes and washed with pre-warmed culture medium before imaging on a Nikon Eclipse TE2000-U (to reduce phototoxicity, lamp fluorescence was limited to 25% and a 0.9 neutral density filter was used). Time-lapse recordings were run immediately after for 5 minutes applying 5-second intervals between time points. Kymographs were obtained using the KymographTracker module available for the Icy image analysis package (copyright Quantitative Image Analysis Unit, Institute Pasteur). A mobile mitochondrion was only considered as such if its dislocation was ≥ 5 µm over the imaging period (Sheng and Cai, 2012).

RT-qPCR of nuclear-encoded mitochondrial genes and qPCR analysis of mitochondrial DNA content

All real-time PCR runs were performed using a LightCycler 480 (software release 1.5, Roche). Triplicate 10-µL reactions were prepared according to manufacturer's instructions (QuantiTect SYBR Green RT-PCR or PCR kits, QIAGEN). RNA purification was performed using RNeasy Mini kit (QIAGEN) and included a DNase-treatment step; QIAamp DNA Micro kit (QIAGEN) was used for DNA purification. Per condition, 7-9 independent samples were collected on different days each consisting of two retinas dissected from the same embryo (stage 37/38). RNA integrity was assessed on a 2100 Bioanalyzer (Agilent) using a Pico assay. For the quantification of nuclear-encoded mitochondrial genes, reference gene (*ywhaz*, tyrosine 3-monooxygenase/tryptophan 5-monooxygenase activation protein, zeta; *rps13*, ribosomal protein S13; *hprt1,* hypoxanthine phosphoribosyltransferase 1; *tbp1,* TATA box binding protein) normalization was performed using

the geNorm module integrated in qbase+ (Biogazelle); the optimal normalization factor was calculated as the geometric mean of reference targets *ywhaz* and *tbp1*; all samples were measured in the same run for a given reference target and data analysis was carried out within qbase+. Real-time quantitative PCR mitochondrial DNA content quantification was accomplished with two different primer sets for genomic (glucagon and beta-2-microglobulin) and mitochondrial (mitochondrially encoded tRNA-leucine and ATP synthase 6) loci; efficiency-corrected run analysis was performed within the LightCycler 480 software. PCR cycling conditions used followed the instructions provided by the manufacturer. See Table 1 for oligonucleotide primer details.

Primary rat cortex neuronal culture and immunocytochemistry

Foetal neurons derived from cortices of F344 rat E18.5 embryos were obtained from Cyagen Biosciences as cryopreserved primary cells, and plated on culture dishes pre-coated with poly-L-lysine (15 µg/mL, Sigma) and laminin (15 µg/mL, incubated overnight at 4ºC, Sigma). Neuronal cultures were grown at 37 ºC in a 5% CO_2 humidified incubator in OriCell Neuron Growth Medium (Cyagen Biosciences) supplemented with L-alanyl-L-glutamine (Life Technologies) and B-27 (Life Technologies) for at least 72 hours before further manipulation. Growth medium was replaced every 36 hours. Immediately before fixation (pre-warmed 4% paraformaldehyde in 1X PBS), cells were washed twice in pre-warmed 1X PBS. After washing the fixative with 10 mM glycine/PBS, cells were permeabilized for 10 minutes with 0.03% Triton X-100 (diluted in PBS). Standard immunocytochemistry protocols were followed henceforth. Blocking solution: 5% heat-inactivated goat serum in 1X PBS; primary antibodies: anti-Tctp (1:400, Santa Cruz Biotechnology; catalog code sc-133131), anti-Mcl1 (1:100, Santa Cruz Biotechnology; catalog code sc-819), and anti-Bcl-X_L (1:100, Santa Cruz Biotechnology; catalog code sc-7195), incubated overnight. Alexa Fluor secondary antibodies (Life Technologies) were used at 1:1000. Laser scanning confocal imaging was performed using an Olympus FV1000 microscope.

In situ proximity ligation assay (PLA)

In situ proximity ligation assays were performed on rat cortex neuronal cultures or HCT116 cells (certified by ATCC) according to manufacturer's recommendations (Duolink; Olink Biosciences, distributed by Sigma). Up until the primary antibodies incubation step, all manipulations were performed as detailed above for the immunocytochemistry procedure. The following primary antibody pairs were used: mouse monoclonal antibody anti-Tctp (1:400, Santa Cruz Biotechnology; catalog code sc-133131) and rabbit polyclonal antibody anti-Mcl1 (1:100, Santa Cruz Biotechnology; catalog code sc-819); mouse anti-Tctp (1:400, Santa Cruz Biotechnology; catalog code sc-133131) and rabbit anti-Bcl-X_L (1:100, Santa Cruz Biotechnology; catalog code sc-7195). Additionally, a blocking Mcl1 peptide (provided by Santa Cruz Biotechnology), used at a five-fold excess relative to the anti-Mcl1 antibody, was included in preliminary experiments to evaluate the specificity of the technique. According to the proprietary information provided by Santa Cruz Biotechnology, the Mcl1 antibody employed is an affinity purified polyclonal antibody raised against a 15-25 long peptide mapping within an internal region (amino acids 100 to 150) of *Homo sapiens* Mcl1 (NCBI accession number Q07820). After overnight primary antibody incubation at 4ºC, all stages of the protocol, except for the washing steps, were performed at 37ºC in a humidity chamber using no more than 100 µL per culture dish. Of note, mouse and rabbit PLA probes were dispensed in blocking solution (5% heat-inactivated goat serum in 1X PBS). All washes prior to the ligation step used PBS; the first round of the last wash steps included Texas Red-Phalloidin (Life Technologies, incubated for 15 minutes at a 1:40 dilution). Cultures were mounted using a minimal volume of Duolink *In Situ* Mounting medium, which incorporates DAPI in its formulation. Image acquisition was performed using an UltraView VoX spinning disk confocal imaging system on an Olympus IX81 microscope.

Quantitative immunofluorescence

Cells were fixed in 2% (vol/vol) paraformaldehyde/7.5% (wt/vol) sucrose for 20 minutes, washed in PBS and permeabilized for 3 minutes using saponin (1 mg/mL in PBS). Standard immunocytochemistry protocols were followed henceforth (blocking solution: 5% heat-inactivated goat serum in 1X PBS). Except for the fixative, a small concentration of saponin (100 µg/mL) was included to reduce the surface tension of all solutions. Fluorescence intensity (mean pixel intensity per unit area) was measured in non-collapsed growth cones with Openlab software (PerkinElmer) or Volocity software (PerkinElmer). Measurements were taken using masks obtained by manually tracing growth cones in corresponding bright-field images. Background fluorescence was then subtracted from total growth cone fluorescence and data were normalized to the mean immunofluorescence intensity of the control group and expressed as percentage. A Nikon Eclipse TE2000-U inverted microscope was used for all image acquisitions. Antibodies: rabbit anti-Tctp (1:500, gift from J. Kubiak); mouse anti-P53 (1:300, Abcam; ab16465); rabbit anti-Active Caspase-3 (1:200, Abcam; ab13847). Alexa Fluor secondary antibodies (Life Technologies) were used at 1:1000.

Table S1. List of PCR oligonucleotide primers

Gene	Primer sequence (5' → 3')	Purpose
tctp	CCACCATACCATCGGGGTTCATTCTTTC	5' RACE
	CAAACACATCCCATCGGGGGTTTC	'Nested' 5' RACE
	GGGATGTGTTTGGAAGTTGAAGGCAAGG	3' RACE
	ACAGGCTTCACCAAGGACTCTTAC	'Nested' 3' RACE
actb	CCTGTGCAGGAAGATCACAT	RT-PCR (axonal RNA purity assessment)
	TGTTAAAGAGAATGAGCCCC	
hist1h4a	AAAAGGACTGGGGAAAGGAGGCGCCA	RT-PCR (axonal RNA purity assessment)
	CGGTCTTCCTCTTGGCGTGTTCTGTG	
map2	CGATCATCCTTGCCAAGACCTTCCTC	RT-PCR (axonal RNA purity assessment)
	GCGACCTGGAGATTGGGTGATGATTT	
tctp coding sequence	TCCAAAGAGAAGAAGGTGCAA	RT-qPCR analysis of *tctp* expression
	CTTGGTGAAGCCTGTTTCCT	
tctp-L unique region	AGAAGCGGACCTTCAGTTTG	RT-qPCR analysis of *tctp* expression
	CCTTCACGGCCAGAAGTATT	
actb	TACTCTTTTGTTGGCGCTTG	RT-qPCR analysis of *tctp* expression (Reference gene)
	GGGCAACACTGAGAGGGTAG	
cox5a	GCCGTCTGCAGTCTGTCTC	Nuclear-encoded mitochondrial gene RT-qPCR
	TCAGTTCCCAGGCATCAATA	
idh3a	TCTTTGCGCAGGTCTAATTG	Nuclear-encoded mitochondrial gene RT-qPCR
	GAAGAAGAGCAGTGGGGTTG	
rhot1 (*miro1*)	TGTACGACGGAGCTAAACCA	Nuclear-encoded mitochondrial gene RT-qPCR
	TTAACATCAGGACCCCAAGG	
cycs	CCTAAGAAGTACATTCCTGGAACAA	Nuclear-encoded mitochondrial gene RT-qPCR
	ATTAACTGGAGGTTGACTGTTTGAG	
hprt1	CCCTGCATTGTGATTCAAGA	Nuclear-encoded mitochondrial gene RT-qPCR (Reference Gene)
	ATATCTCGAGCCAGCCTTTC	

Table S1 (continued). List of PCR oligonucleotide primers

tbp1	GAAGAAAGCTGGTCAACAGGA GGGACTCCTTACAGTACCCAGA	Nuclear-encoded mitochondrial gene RT-qPCR (Reference Gene)
rps13	CTTCAAACTGGCCAAGAAGG GGCCAGAGCCTTAGACTTGA	Nuclear-encoded mitochondrial gene RT-qPCR (Reference Gene)
gcg	TGATTCAGAACAGCTCAAGGAA AGCCCGTCTGGAGTCTAGGTA	Mitochondrial DNA Content Analysis (Nuclear DNA)
b2m	AATGAGGTGATCTGCTACGTGT TTCCAGTTATGTTGGAATGAGG	Mitochondrial DNA Content Analysis (Nuclear DNA)
ATP synthase F0 subunit 6	CCTGAAGGAACACCAACACC TAGCAGTAAGTCGAACTCCAAGG	Mitochondrial DNA Content Analysis (Mitochondrial DNA)
mtDNA-tRNA-leucine	AATAGGGCATTAGCGACAGC GTGGCATATCATTAAGGGTGGT	Mitochondrial DNA Content Analysis (Mitochondrial DNA)
pgc1a	ATCTGGGTGTTGATCCAAGTGACG CAGTCCCCAGTCACATGACAAAGC	*Homo sapiens pgc1a* promoter cloning

SUPPLEMENTAL REFERENCES

Agathocleous, M., Love, N. K., Randlett, O., Harris, J. J., Liu, J., Murray, A. J. and Harris, W. A. (2012). Metabolic differentiation in the embryonic retina. *Nature cell biology* **14**, 859-864.

Amson, R., Pece, S., Lespagnol, A., Vyas, R., Mazzarol, G., Tosoni, D., Colaluca, I., Viale, G., Rodrigues-Ferreira, S., Wynendaele, J., et al. (2012). Reciprocal repression between P53 and TCTP. *Nature medicine* **18**, 91-99.

Bassell, G. J., Zhang, H., Byrd, A. L., Femino, A. M., Singer, R. H., Taneja, K. L., Lifshitz, L. M., Herman, I. M. and Kosik, K. S. (1998). Sorting of beta-actin mRNA and protein to neurites and growth cones in culture. *The Journal of neuroscience : the official journal of the Society for Neuroscience* **18**, 251-265.

Falk, J., Drinjakovic, J., Leung, K. M., Dwivedy, A., Regan, A. G., Piper, M. and Holt, C. E. (2007). Electroporation of cDNA/Morpholinos to targeted areas of embryonic CNS in Xenopus. *BMC developmental biology* **7**, 107.

Leung, L. C., Urbancic, V., Baudet, M. L., Dwivedy, A., Bayley, T. G., Lee, A. C., Harris, W. A. and Holt, C. E. (2013). Coupling of NF-protocadherin signaling to axon guidance by cue-induced translation. *Nature neuroscience* **16**, 166-173.

Livak, K. J. and Schmittgen, T. D. (2001). Analysis of relative gene expression data using real-time quantitative PCR and the 2(-Delta Delta C(T)) Method. *Methods* **25**, 402-408.

Love, N. K., Keshavan, N., Lewis, R., Harris, W. A. and Agathocleous, M. (2014). A nutrient-sensitive restriction point is active during retinal progenitor cell differentiation. *Development* **141**, 697-706.

Marks, J. D., Boriboun, C. and Wang, J. (2005). Mitochondrial nitric oxide mediates decreased vulnerability of hippocampal neurons from immature animals to NMDA. *The Journal of neuroscience : the official journal of the Society for Neuroscience* **25**, 6561-6575.

Nieuwkoop, P. D. and Faber, J. (1994). *Normal table of Xenopus laevis (Daudin) : a systematical and chronological survey of the development from the fertilized egg till the end of metamorphosis*. New York: Garland Pub.

Pfaffl, M. W. (2001). A new mathematical model for relative quantification in real-time RT-PCR. *Nucleic acids research* **29**, e45.

Sahin, E., Colla, S., Liesa, M., Moslehi, J., Muller, F. L., Guo, M., Cooper, M., Kotton, D., Fabian, A. J., Walkey, C., et al. (2011). Telomere dysfunction induces metabolic and mitochondrial compromise. *Nature* **470**, 359-365.

Sheng, Z. H. and Cai, Q. (2012). Mitochondrial transport in neurons: impact on synaptic homeostasis and neurodegeneration. *Nature reviews. Neuroscience* **13**, 77-93.

Wareski, P., Vaarmann, A., Choubey, V., Safiulina, D., Liiv, J., Kuum, M. and Kaasik, A. (2009). PGC-1{alpha} and PGC-1{beta} regulate mitochondrial density in neurons. *The Journal of biological chemistry* **284**, 21379-21385.

Xue, X. Y. and Harris, W. A. (2012). Using myc genes to search for stem cells in the ciliary margin of the Xenopus retina. *Developmental neurobiology* **72**, 475-490.

Zivraj, K. H., Tung, Y. C., Piper, M., Gumy, L., Fawcett, J. W., Yeo, G. S. and Holt, C. E. (2010). Subcellular profiling reveals distinct and developmentally regulated repertoire of growth cone mRNAs. *The Journal of neuroscience : the official journal of the Society for Neuroscience* **30**, 15464-15478.